ARTICLES

Subunit arrangement and function in NMDA receptors

Hiroyasu Furukawa[1]†, Satinder K Singh[1]†, Romina Mancusso[1]† & Eric Gouaux[1,2]†

Excitatory neurotransmission mediated by NMDA (*N*-methyl-D-aspartate) receptors is fundamental to the physiology of the mammalian central nervous system. These receptors are heteromeric ion channels that for activation require binding of glycine and glutamate to the NR1 and NR2 subunits, respectively. NMDA receptor function is characterized by slow channel opening and deactivation, and the resulting influx of cations initiates signal transduction cascades that are crucial to higher functions including learning and memory. Here we report crystal structures of the ligand-binding core of NR2A with glutamate and that of the NR1–NR2A heterodimer with glutamate and glycine. The NR2A–glutamate complex defines the determinants of glutamate and NMDA recognition, and the NR1–NR2A heterodimer suggests a mechanism for ligand-induced ion channel opening. Analysis of the heterodimer interface, together with biochemical and electrophysiological experiments, confirms that the NR1–NR2A heterodimer is the functional unit in tetrameric NMDA receptors and that tyrosine 535 of NR1, located in the subunit interface, modulates the rate of ion channel deactivation.

Glutamate, a simple amino acid, is an essential currency of the human nervous system and is transmitted from one neuron to another at specialized junctions called synapses. The tightly regulated release of glutamate from one neuron, coupled with its detection by glutamate receptors on the adjacent neuron, forms the basis of synaptic transmission at many of the $\sim 10^{14}$ synapses in the human brain[1]. Specificity of synaptic signalling by glutamate in space and time is conferred by the precise positioning of synapses and by the neuron-specific expression of a subset of genes encoding glutamate receptors. Pharmacological studies provided initial clues to the diversity of glutamate receptor proteins, and early studies partitioned them into two classes depending on their response to the synthetic agonist NMDA[2]. Subsequent cloning of glutamate receptor genes and analysis of their predicted protein sequences facilitated the clustering of NMDA and non-NMDA receptors into distinct protein familes[3–7].

NMDA receptors are unusual ligand-gated ion channels because activation not only requires the binding of two agonists, glycine and glutamate[8], but also demands the relief of Mg^{2+} block by membrane depolarization[9]. The opening of NMDA receptors leads to an influx of cations including Ca^{2+}, and the permeation of Ca^{2+} through NMDA receptor ion channels[10] initiates signal transduction cascades that in turn modulate synaptic strength. The rates at which the responses of NMDA receptors rise (activate) and decline (deactivate) upon application and removal of agonists, respectively, are markedly slower than those of non-NMDA receptors[11,12] and it is the slow deactivation rate of NMDA receptors that governs the duration of the excitatory postsynaptic potential, a measure of the 'strength' of synaptic signalling[13]. The integration of chemical and electrical stimuli by NMDA receptors into a Ca^{2+} signal is crucial for activity-dependent synaptic plasticity, which in turn underpins many higher functions including learning and memory. By contrast, dysfunction of NMDA receptors has been implicated in many diseases and injuries including stroke, Parkinson's disease, Huntington's disease and schizophrenia[14,15].

The functional diversity shown by NMDA receptors is rooted in their assembly as obligate heteromers of glycine-binding NR1, glutamate-binding NR2 and glycine-binding NR3 subunits. Whereas non-NMDA receptors such as AMPA (α-amino-3-hydroxy-5-methyl-4-isoxazole propionic acid) and kainate receptors can form functional homotetrameric channels activated solely by glutamate, NMDA receptors require the assembly of two copies each of the NR1 and NR2 and/or NR3 subunits[16,17]. Contingent on the cell and the developmental stage, typically one of the four NR2 subunits (A–D) combines with a splice variant of the NR1 subunit, yielding receptors with distinct deactivation kinetics[18,19]. The apparent affinity of the NR1 subunit for glycine depends on the identity of the coassembled NR2 subunit, which suggests that there is allosteric coupling between NR1 and NR2[20]. Moreover, for a particular combination of NR1 and NR2 subunits, glycine and glutamate binding show negative cooperativity, giving rise to a glycine-dependent form of receptor desensitization[21].

Studies of AMPA receptors have shown that the receptor subunits assemble as a dimer of dimers through interactions between different domains on each subunit, including the amino terminal domain (ATD) and the ligand-binding domain (S1S2)[22] (Fig. 1a), and dimers of the ligand-binding domain of the GluR2 receptor have been particularly well studied[23,24]. Although it has been speculated that NMDA receptors are also organized as a dimer of dimers with an NR1–NR1–NR2–NR2 arrangement[25] mediated by the ATD[26] and part of the S1 segment[27], conclusive proof of the subunit arrangement and the nature of subunit–subunit contacts is lacking (Fig. 1b). In addition, mechanistic understanding of the role that subunit–subunit contacts might have in NMDA receptor activity is absent.

Here we present crystal structures of the ligand-binding core of NR2A bound to glutamate and that of the NR1–NR2A heterodimer bound to glycine and glutamate. The physiological relevance of the subunit arrangement observed in the NR1–NR2A crystal structure is confirmed by biochemical and electrophysiological experiments. Significantly, detailed analysis of the NR1–NR2A ligand-binding

[1]Department of Biochemistry and Molecular Biophysics and [2]Howard Hughes Medical Institute, Columbia University, 650 West 168th Street, New York, New York 10032, USA. †Present addresses: Vollum Institute, Oregon Health and Science University, Portland, Oregon 97239, USA (H.F., S.K.S., E.G.); The Structural Biology Program, Memorial Sloan-Kettering Cancer Center, 1275 York Avenue, New York, 10021, USA (R.M.).

core identifies a site in the heterodimer interface that has a key role in modulating the rate of receptor deactivation.

Structures of the ligand-binding cores

NMDA receptors are modular proteins, and the ligand-binding S1S2 domain can be prepared as a water-soluble protein that binds agonists and antagonists with affinities similar to those of the full-length assembled receptors[28] (Fig. 1). In the AMPA subtype of glutamate receptor, the GluR2 S1S2 domain participates in key subunit–subunit contacts in the intact receptor. To understand the molecular basis for intersubunit interactions in NMDA receptors, we solved structures of the NR2A S1S2 domain bound to glutamate (Supplementary Table S1 and Fig. S1) and the NR1–NR2A S1S2 complex bound to glycine and glutamate (Fig. 2 and Supplementary Table S1). Together with previously determined structures of NR1 S1S2 (refs 28, 29), we now have atomic-scale views of the glycine- and glutamate-binding sites and, most importantly, we have the structure of the NR1–NR2A S1S2 heterodimer.

The NR1–NR2A S1S2 heterodimer crystallizes as a single complex in the asymmetric unit with the two subunits related by a pseudo two-fold axis located at the centre of the interface (Fig. 2). The heterodimer buries 2,640 Å^2 of solvent-accessible surface area, and the sites of subunit–subunit contact can be divided into three subsites: sites I and III are related by the pseudo two-fold axis, and site II is on the pseudo two-fold axis (Fig. 2). Site II includes Y535 and P532 of NR1, P527 of NR2A, a salt bridge between R755 of NR1 and E530 of NR2A, and a hydrogen bond between K531 of NR1 and the backbone carbonyl oxygen of F524 of NR2A (Fig. 2d). Sites I and III comprise primarily hydrophobic residues on helices D and J of domain 1 and include I519, A524 and L777 of NR1 and I514, V526, L777 and L780 of NR2A (Fig. 2c, e). Sites I and III also include several polar contacts, not only between domain 1 of each subunit but also between domain 1 (helix J) and domain 2 (helix F). Because agonist binding results in lobe closure and movement of domain 2, the intersubunit contacts between domain 1 and domain 2, which are not seen in the GluR2 S1S2 dimer[23,24,30], provide a mechanism by which the binding of agonists can be coupled to the interactions between subunits, that is, to the dimer interface[21].

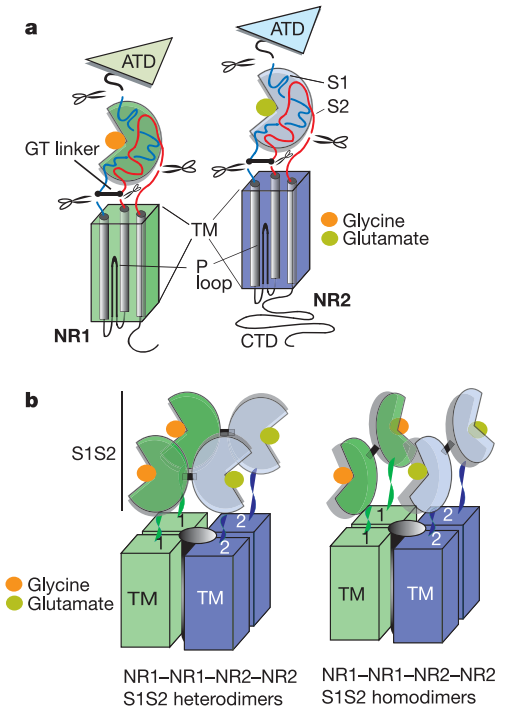

Figure 1 | Oligomeric arrangement in NMDA receptors. a, Domain organization of NMDA receptor subunits. Both NR1 and NR2 consist of N- (ATD) and C- (CTD) terminal domains, a transmembrane domain (TM) and a S1S2 ligand-binding core. The ligand-binding core can be isolated by tethering S1 and S2 with a Gly–Thr (GT) dipeptide linker. **b**, NMDA receptors form tetrameric channels comprising two copies each of NR1 and NR2. Shown here are the two possible modes of dimerization at the S1S2 ligand-binding cores, assuming that the subunits are organized in a NR1–NR1–NR2–NR2 arrangement[25]. Thick black lines between the S1S2 domains indicate the formation of a particular homo- or heterodimer interface. ATD and CTD have been omitted for clarity.

The subunits in the NR1–NR2A S1S2 heterodimer are arranged in a 'back-to-back' fashion that is similar to the arrangement of subunits in the non-desensitized state of the GluR2 S1S2 homodimer[23,24]. Indeed, domain 1 of each subunit of the heterodimer superimposes with a root-mean-square (r.m.s.) deviation of 0.9 Å onto the 256 corresponding Cα atoms of the GluR2 S1S2–glutamate structure[23] (Fig. 2f, g). By contrast, domain 2 of the NR1–NR2A S1S2 and the GluR2 S1S2 structures superimpose poorly owing to differences in domain closure and the structural organization of domain 2 (Fig. 2f). Nevertheless, the similar subunit arrangement in the NR1–NR2A S1S2 heterodimer and the GluR2 S1S2 homodimer has three important implications.

First, it shows that the basic arrangement and interactions of subunits in the ligand-binding cores is conserved between NMDA receptors and non-NMDA receptors. Second, because the S1S2 dimer interface is a crucial site for receptor modulation in GluR2 (ref. 24), it is plausible that the heterodimer interface in NR1–NR2A is a locus for NMDA receptor modulation. Third, the conserved architecture suggests that gating of the ion channel in NMDA receptors occurs by a mechanism similar to that in non-NMDA receptors; that is, closure of each ligand-binding core 'clam shell' results in separation of the linker regions proximal to the ion channel domain. Notably, the separation of the equivalent 'linker' positions in the NR1–NR2A–glycine–glutamate complex is ~32 Å, whereas this distance in the GluR2–glutamate complex is ~38 Å. The molecular basis for this difference stems from disparities in the conformations of domain 2 and in the extent of domain closure between the NR1–NR2A and GluR2 S1S2 structures.

Glutamate-binding site of NR2A

The crystal structure of the NR2A ligand-binding core reveals recognition elements for glutamate and suggests a mechanism by which the NR2 subunits bind NMDA (Supplementary Fig. S1). On comparing the agonist-binding site of NR2A with the corresponding site of GluR2 (refs 23, 30, 31), GluR5 (ref. 32) and GluR6 (refs 32, 33), we find that the crucial difference is a negatively charged residue that participates in binding the positively charged amino group of the agonist. In NR2A this residue is D731, whereas in non-NMDA receptors the equivalent residue is a glutamate. Because the aspartate present in NR2A is one methylene group shorter than the glutamate present in non-NMDA receptors, there is no salt bridge between D731 and the amino group of the agonist glutamate as there is in non-NMDA receptors (Supplementary Fig. S1c). In NR2A, the amino group of the agonist forms water-mediated hydrogen bonds to residues E413 and Y761 (Supplementary Fig. S1b). Because the NR2 subunits have the shorter aspartate residue, NMDA can be modelled into the agonist-binding pocket by displacing the water molecule W2 (Supplementary Fig. S1d). If a similar exercise is carried out in the context of GluR2, steric clash occurs between the *N*-methyl group and the glutamate residue of the receptor.

A second feature of the binding site in NR2A that is distinct from non-NMDA receptors is a van der Waals contact between the γ-carboxylate group of glutamate and Y730, a residue that is conserved among NR2 subunits (Supplementary Fig. S1b). This contact, as well as an interdomain hydrogen bond between Y730 and E413, may partially account for the high-affinity binding of glutamate to NMDA receptors. Accordingly, mutation of the equivalent tyrosine in NR2B to alanine increases by 450-fold

the effector concentration for half-maximum response (EC_{50}) for glutamate[34]. Despite differences in the pharmacology of glutamate binding and in the architectures of the glutamate-binding pockets, both NMDA receptors and non-NMDA receptors bind glutamate in the 'folded' rather than the 'extended' conformation, as suggested previously[35].

Physiological arrangement of NR1 and NR2A subunits

To validate the relevance of the NR1–NR2A subunit arrangement observed in the crystal to the intact receptor, we carried out biochemical, electrophysiological and sedimentation studies. We first engineered double cysteine mutants into both NR1 and NR2A by using the heterodimer crystal structure as a guide. Cysteines introduced at N521 and L777 of NR1 and E516 and L780 of NR2A, sites related by the pseudo two-fold axis, are predicted to form unstrained disulphide bonds across the heterodimer interface (Fig. 3a). We reasoned that if the heterodimer interface is present in the intact receptor, then coexpression of the double cysteine mutants should result in crosslinked NR1 and NR2A subunits. By contrast, coexpression of the wild-type subunits, or subunits with only one set of double cysteine mutations, should not give rise to a disulphide-linked dimer.

Coexpression of wild-type subunits (WT–WT), NR1 double cysteine mutant and NR2A wild-type subunits (M–WT), or NR1 wild-type and NR2A double cysteine mutant subunits (WT–M) gave rise to bands that migrated as monomers under both reducing and non-reducing conditions (Fig. 3b). However, coexpression of the NR1 double cysteine mutant and NR2A double cysteine mutant

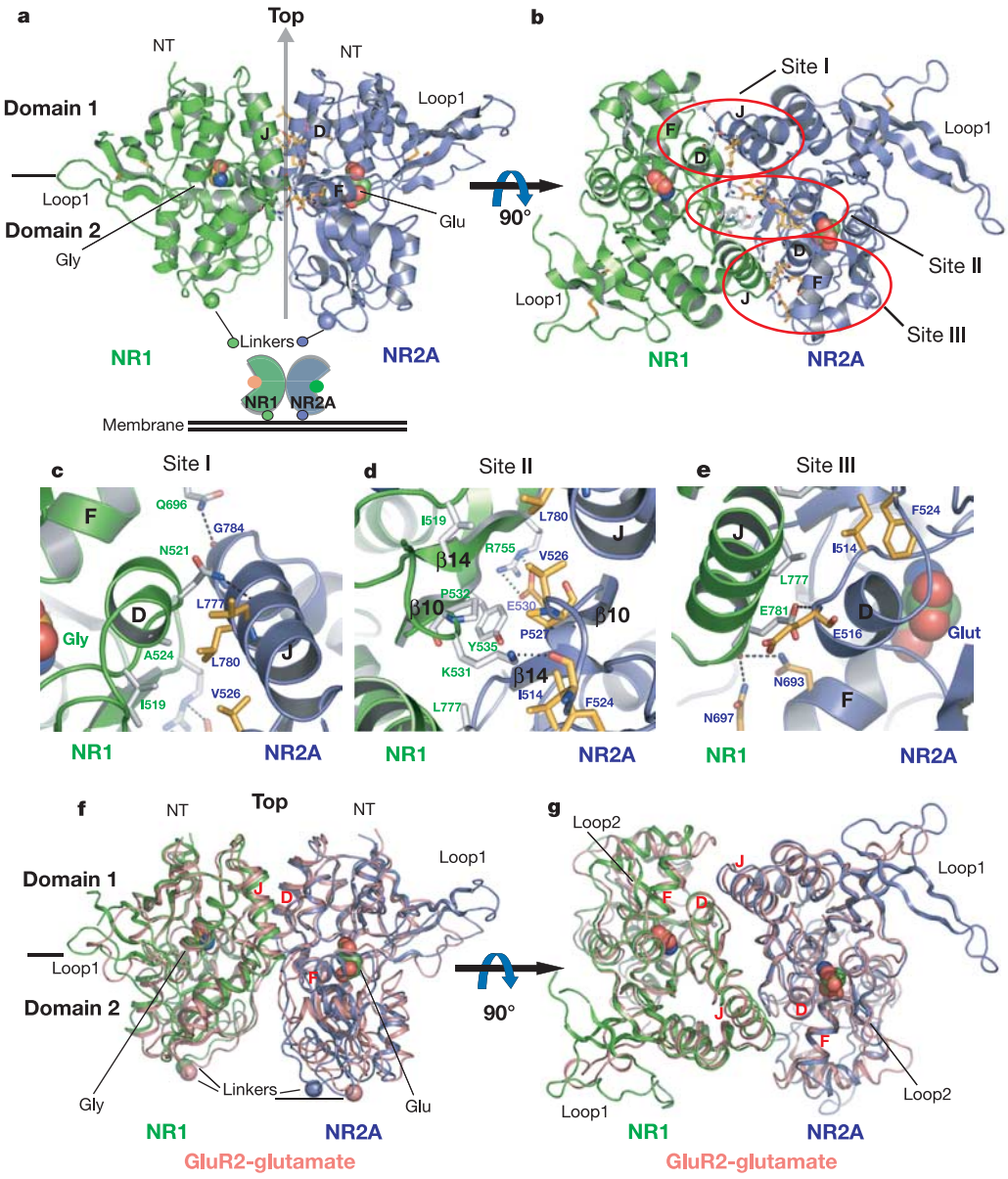

Figure 2 | Structure of NR1–NR2A S1S2. a, Side view of the NR1–NR2A S1S2 heterodimer in complex with glycine and glutamate. NR1 and NR2A are coloured green and blue, respectively. Glycine, glutamate and the Cα atom of the glycine residue in the Gly–Thr dipeptide linker are shown as spheres. The arrow indicates the pseudo two-fold axis between the protomers. **b**, View of the structure from the 'top'. The interface between NR1 and NR2A is sliced into three sections denoted sites I–III. **c**–**e**, Magnified view of the interactions at sites I, II and III. Dashed lines indicate hydrogen bonds or salt bridges. The interacting residues from NR1 and NR2A are coloured white and orange, respectively. **f**, **g**, Structural comparison between the NR1–NR2A (green–blue) S1S2 heterodimer and the glutamate-bound GluR2 S1S2 (pink) homodimer (PDB code 1FTJ). Superimposed structures are viewed from the side and 'top' of the molecules in **f** and **g**, respectively. Superposition was carried out on 256 residues from domain 1 with the program LSQKAB[50]. The Cα atoms of the glycine residues in the Gly–Thr dipeptide linkers are shown as spheres.

subunits (M–M) gave rise to a prominent band at a relative molecular mass of ~300,000 ($M_r \approx 300$K) that was recognized by antibodies against both NR1 and NR2A and was observed only under non-reducing conditions. We suggest that the ~300K band corresponds to a spontaneously disulphide-linked NR1–NR2A heterodimer, in which the disulphide bridges form across the heterodimer interfaces of the S1S2 ligand-binding cores.

To determine whether the engineered cysteine residues affected the gating behaviour of the receptor, we measured ion channel activity for all wild-type and mutant combinations by two-electrode voltage clamp (TEVC). Application of glycine and glutamate elicited currents for all subunit combinations, indicating that the cysteine mutations did not disrupt receptor function. Application of 2 mM DTT for 1 min slightly potentiated the current induced by glutamate and glycine in the WT–WT channel, the effect of which was most probably due to reduction of the NR1 C744–C798 disulphide bond[36]. Similar effects were seen in the WT–M and M–WT channels. By contrast, DTT significantly potentiated the current in the M–M channel (Fig. 3c). The extent of this potentiation was greater than the sum of the effects in the WT–M and M–WT channels, indicating that it was specific to the M–M combination of receptor subunits. Because the M–M combination gave rise to both a heterodimer band under non-reducing conditions in western blotting and the greatest DTT-mediated potentiation in the TEVC experiments, we propose that the arrangement of subunits in the NR1–NR2A S1S2 crystal structure is similar to that in the intact NR1–NR2A NMDA receptor.

To probe further the NR1–NR2A heterodimer interface, we measured the homo- and heterodimerization propensities of NR1 and NR2A S1S2 constructs by size-exclusion chromatography coupled to light scattering, refractive index and ultraviolet measurements (SEC-LS/RI/UV)[37], combined with sedimentation equilibrium and velocity experiments (Fig. 4 and Supplementary Fig. S2). We found that wild-type NR1, NR2A or an equimolar mixture of NR1–NR2A S1S2 did not oligomerize to an appreciable extent, even at concentrations of up to 3 mg ml^{-1} (Fig. 4d and Supplementary Fig. S2 and Table S2), similar to the behaviour of the wild-type GluR2 S1S2 ligand-binding core[24]. In GluR2, however, the mutation of L483 to tyrosine enhances S1S2 dimerization by 10^5-fold and greatly slows receptor desensitization[38]. Because the NR1–NR2A and GluR2 dimer interfaces are similar, we reasoned that by introducing tyrosine residues into the NR1 and NR2A subunits at positions equivalent to L483 in GluR2, we might be able to study the oligomerization behaviour of the NMDA receptor ligand-binding cores at protein concentrations amenable to light scattering and sedimentation analyses.

As predicted, the association pattern of the S1S2 proteins were altered by the introduction of these tyrosine residues (N521Y in NR1 and E516Y in NR2A), while ion channel activity was not significantly perturbed, as measured by TEVC (Supplementary Fig. S3 and Table S3). Specifically, SEC-LS/RI/UV and sedimentation equilibrium experiments showed that NR1 S1S2 N521Y dimerized with a dissociation constant of approximately 0.7 mg ml^{-1} (Fig. 4e, f and Supplementary Table S2), whereas NR2A S1S2 E516Y remained exclusively monomeric at concentrations up to 1.2 mg ml^{-1} (Fig. 4e, g, and Supplementary Table S2). However, when NR2A S1S2 E516Y was mixed with an equimolar ratio of NR1 S1S2 N521Y at a total protein concentration of 0.8 mg ml^{-1} and examined by SEC-LS/RI/UV, only a dimeric species was observed (Fig. 4e). The dramatic change in the association behaviour of NR2A S1S2 E516Y in the presence of NR1 S1S2 N521Y indicates that the NR2A ligand-binding core preferentially forms a heterodimer with the NR1 ligand-binding core. These results, together with the disulphide crosslinking and electrophysiological data, reinforce the conclusion that the NR1–NR2A arrangement seen in the crystal structure is present in the full-length receptor.

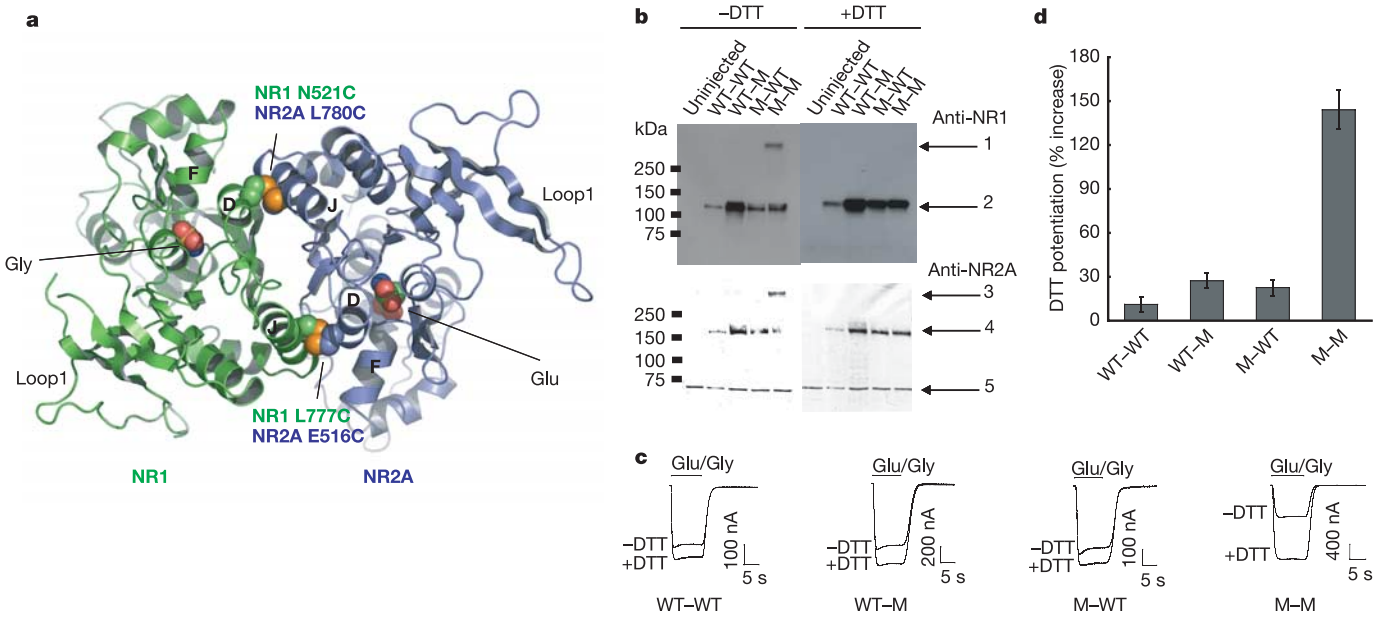

Figure 3 | Engineering disulphide bonds at the NR1–NR2A heterodimer interface. **a**, Location of the cysteines (spheres) engineered on helices D and J at positions N521 and L777 in NR1 and E516 and L780 in NR2A. **b**, Assessment of disulphide bond formation by western blot. Membrane fractions of *Xenopus* oocytes expressing different combinations of wild-type (WT) and mutant (M) NR1–NR2A channels (WT–WT, M–WT, WT–M and M–M) were probed by antibodies against NR1 or NR2A in the presence or absence of DTT. Higher M_r species (arrows 1 and 3), representing the NR1–NR2A heterodimer, are seen only in the M–M lane ((DTT), and monomers (arrows 2 and 4) are seen in all of the other lanes (±DTT). Bands indicated by arrow 5 are nonspecific background. Enhanced chemiluminescence and alkaline phosphatase methods were used to detect bands on the anti-NR1 and anti-NR2A blots, respectively. **c**, **d**, Current recordings of the mutant channels in the presence of 300 μM glycine and 300 μM glutamate and in the presence or absence of DTT (2 mM for 1 min) by TEVC at −60 mV. On application of DTT significant potentiation (~140% increase) was observed in the M–M channel ($n = 9$, $P < 0.001$), whereas only a small effect was observed in the WT–WT ($n = 4$), WT–M ($n = 6$) and M–WT ($n = 5$) channels. No significant run down was detected in the experiment. Error bars in **d** represent the s.d.

Site II in heterodimer interface modulates deactivation

The structural parallels between the NR1–NR2A S1S2 heterodimer and the GluR2 S1S2 homodimer suggest that specific regions in the intersubunit interface may have similar functions. Analysis of the GluR2 dimer interface shows that the regions corresponding to sites I and III (Fig. 2), namely the contacts between helix D on one subunit and helix J on the other, are involved in modulating receptor desensitization[24]. By contrast, the region equivalent to site II (Figs 2 and 5) in AMPA receptors defines the binding site of small molecules, such as aniracetam, that modulate receptor deactivation[39] by stabilizing the ligand-binding domain in a closed-cleft, activated conformation. Interdomain hydrogen bonds stabilize a closed-cleft conformation[23,32], but binding of a modulator also does so by locking the 'clam shell' hinge[39]. Comparison of site II in the NR1–NR2A S1S2 interface with the equivalent region in GluR2 shows that key conserved proline residues, P532 (NR1) and P527 (NR2A), are located in positions similar to those of the prolines in GluR2 (P494). Furthermore, the superposition shows that the aromatic ring of Y535 in NR1 occupies a position in the heterodimer equivalent to that of aniracetam in the GluR2 homodimer (Fig. 5), namely at the hinge of the ligand-binding core clam shell. Specifically, the aromatic ring and hydroxyl group of NR1 Y535 overlap with one edge of the benzoyl ring and the adjacent edge of the pyrrolidinone ring of aniracetam, and the hydroxyl group of Y535 superimposes with the benzoyl carbonyl oxygen. Consequently, the tyrosine ring of NR1 Y535 and aniracetam in the GluR2 complex are involved in analogous interactions with their respective receptors. Because Y535 occupies a similar position in a NR1/NR2A heterodimer as aniracetam occupies in a GluR2 homodimer, we hypothesize that residue 535 modulates deactivation in NMDA receptors.

To test the role of NR1 Y535 in modulating NMDA receptor deactivation, we individually mutated this tyrosine to alanine, serine, leucine, phenylalanine and tryptophan, expressed the resulting receptor variants in HEK293 cells, and determined the rates of glycine- and glutamate-dependent deactivation by patch-clamp, rapid-solution-exchange measurements. For the wild type and all of the mutants, the rates of glycine and glutamate deactivation after brief applications of agonist were fit by a double exponential expressed with a fast (τ_f) and a slow (τ_s) component (Fig. 6 and Supplementary Table S4).

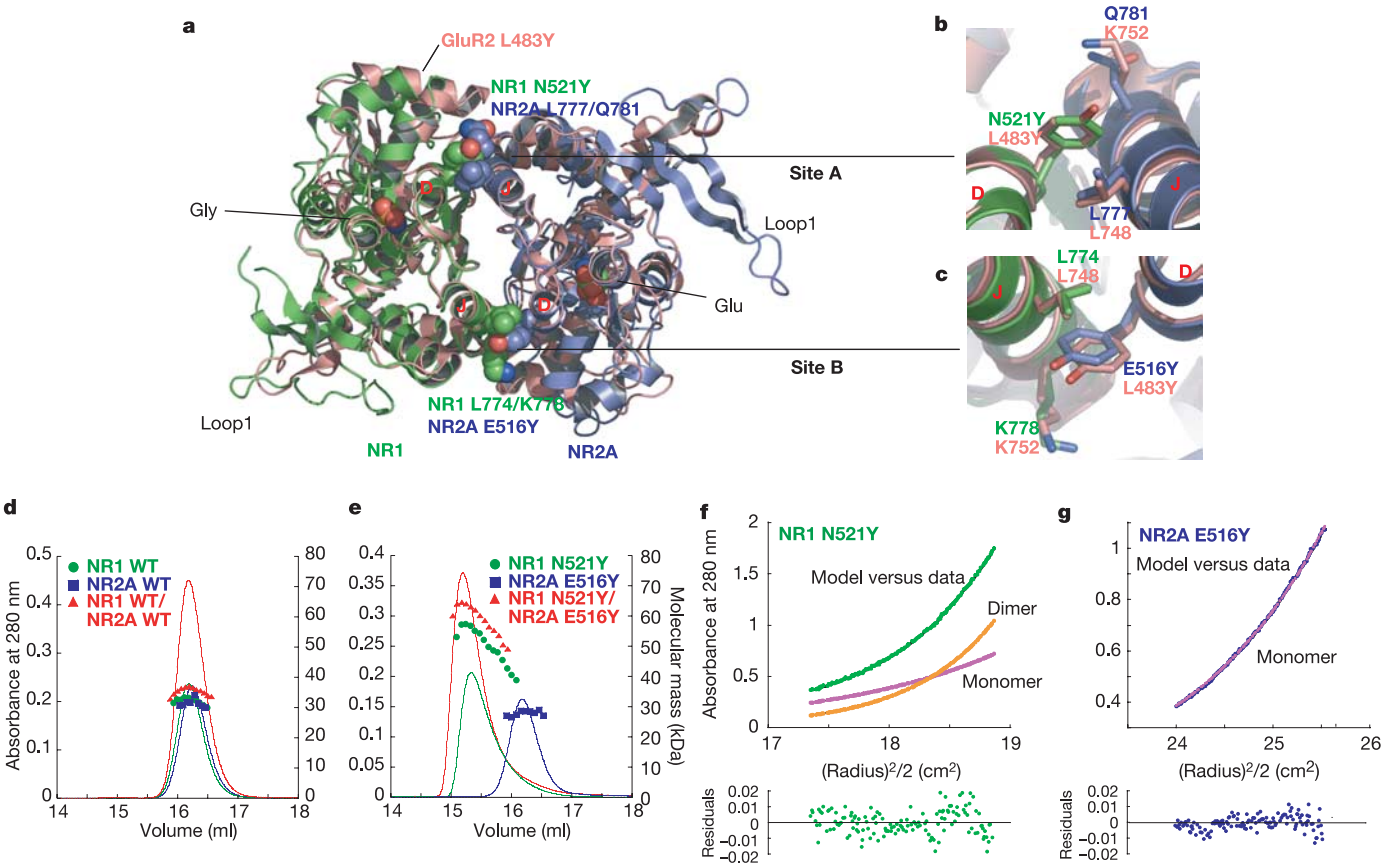

Figure 4 | Heterodimerization is favoured in NR1 S1S2 N521Y and NR2A S1S2 E516Y. a, Superposition of the GluR2 S1S2 L483Y (pink) homodimer onto the NR1–NR2A S1S2 (green–blue) heterodimer. The mutations N521Y in NR1 and E516Y in NR2A were designed using the GluR2 S1S2 L483Y structure (PDB code 1LB8) as a guide. **b**, **c**, Putative contacts at sites A and B in the NR1–NR2A mutant involve hydrophobic and cation–π interactions similar to those observed in GluR2 L483Y. **d**, **e**, Mass analysis by SEC-LS/RI/UV. The calculated M_r values are plotted for NR1 alone, NR2A alone and an equimolar mixture of NR1 and NR2A for both wild-type (**d**) and mutant (**e**) receptors. Solid lines represent the SEC profiles observed by absorbance at 280 nm. Dimeric and monomeric species form with NR1 S1S2 N521Y alone or with an equimolar mixture of NR1 S1S2 N521Y and NR2A S1S2 E516Y, whereas only monomeric species form with NR2A S1S2 E516Y or wild-type receptors. The concentration of all samples was 0.8 mg ml^{-1}. **f**, **g**, Sedimentation equilibrium analysis of NR1 S1S2 N521Y (**f**) and NR2A S1S2 E516Y (**g**). Scans from three concentrations (0.2, 0.4 and 0.8 mg ml^{-1}) and three rotor speeds (13,000, 18,000 and 25,000 r.p.m.) were globally fit to either a monomer–dimer (NR1) or a single-species monomer (NR2A) model. Floating the reduced molecular weights yielded an M_r of 32.9K and 31.6K for the NR1 and NR2A monomers, respectively, which are within 1.5% of the values expected from their amino acid sequences disregarding disulphide bonds. Black lines indicate the model used to fit the data; green (NR1 N521Y) and blue (NR2A E516Y) circles indicate actual measurements; purple and orange lines represent the respective proportions of monomer and dimer calculated from the models. The graphs show the species distribution for the 0.8 mg ml^{-1} samples at 13,000 r.p.m. Residuals in absorbance units are shown below each graph.

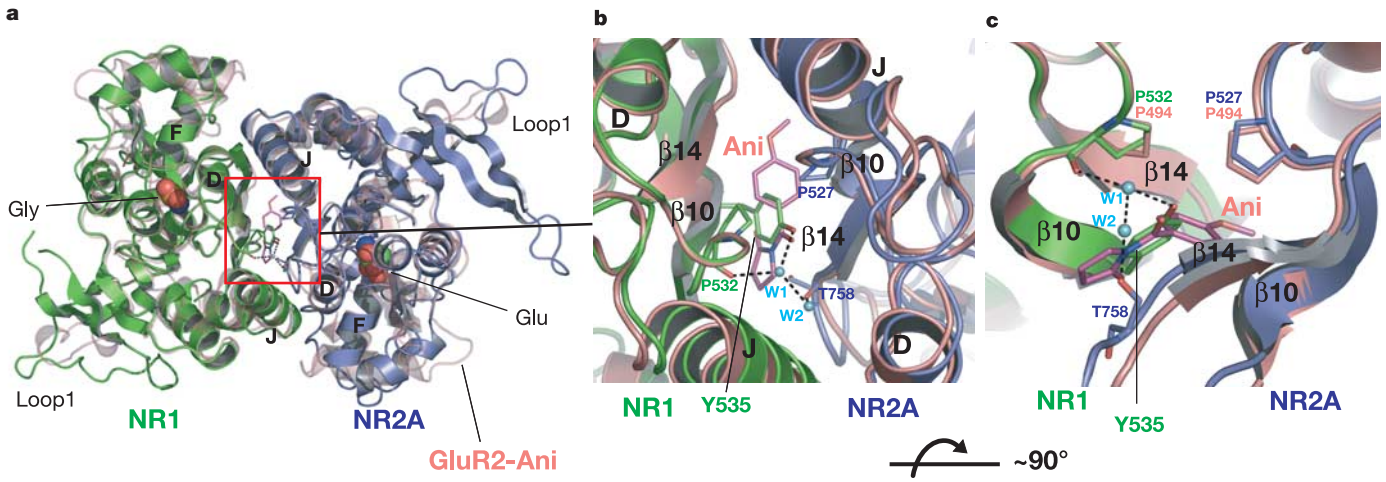

Figure 5 | Superposition of NR1–NR2A S1S2 and the GluR2 S1S2–aniracetam complex. **a**, Overlay of the GluR2 S1S2 dimer bound to glutamate and aniracetam (Ani, pink) onto the NR1–NR2A S1S2 dimer (green and blue) viewed from the same angle as in Fig. 1b. **b**, Magnification of the NR1 Y535 site and the aniracetam-binding site viewed from the same angle as in **a**. Two water molecules, W1 and W2 (cyan spheres), participate in stabilizing the NR1–NR2A interaction. **c**, Side view of the NR1 Y535 site. Note that the position of the aniracetam molecule (pink) overlaps with that of the aromatic side chain of NR1 Y535.

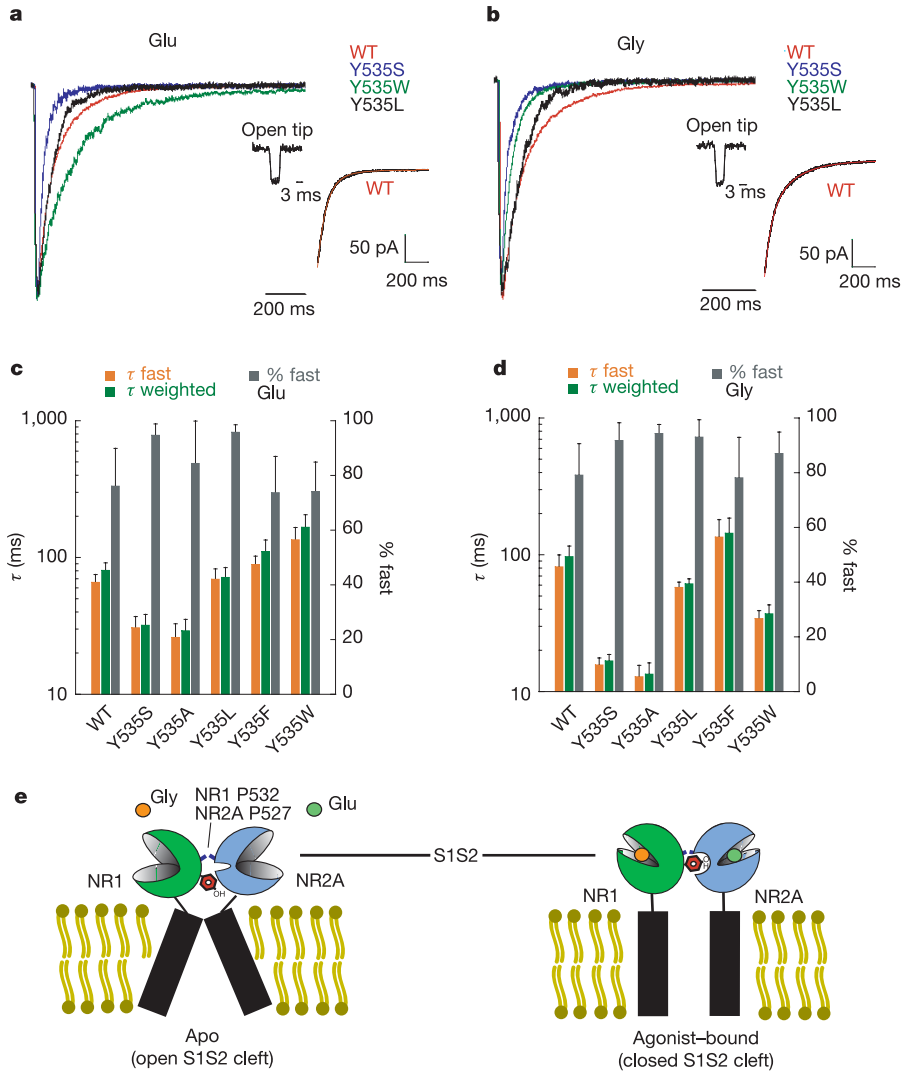

Figure 6 | Residue NR1 Y535 modulates the rate of NMDA receptor deactivation. **a**, **b**, Normalized traces of glutamate- (**a**) or glycine- (**b**) induced currents for NR1 Y535S, Y535W, Y535L and wild-type (WT) combined with wild-type NR2A. Insets show the fit of the wild-type current decays to a double exponential equation after a 3-ms application of ligand (traces are shown in black and equation fits in red; see Methods). The typical open-tip response is roughly 500 μs for a rise from 10 to 90%. **c**, **d**, Time constant values (τ) and percentages of the fast components of deactivation for glutamate- and glycine-induced currents calculated from the double exponential fit. Bars show mean ±s.d. from ten different patches. Note that the y axis for τ is on a log scale. **e**, Proposed mechanism by which Y535 of the NR1 subunit (red) slows the deactivation of NMDA receptors. The aromatic side chain of Y535 binds to a primarily hydrophobic pocket at the hinge region of the NR2A subunit, stabilizing the activated, glutamate-bound conformation. A single heterodimer with S1S2 and transmembrane domains is shown for clarity.

Mutation of NR1 Y535 to alanine or serine results in an increase in the rates of deactivation for glycine and glutamate by as much as 5–7-fold (Fig. 6c, d), owing more to an increase in the fast deactivation component (τ_f) and its relative weight (% fast) and less to a change in the rate of the slow component (τ_s). In AMPA receptors, the rate of deactivation is about two orders of magnitude greater than that in the NR1–NR2A NMDA receptor and the residue equivalent to NR1 Y535 is a serine, which suggests that the shape and volume of the residues at this position modulate the rate of receptor deactivation. The increase in the rate of glycine deactivation for the NR1 Y535S mutant is due, at least in part, to the fact that this mutant has a lower affinity or a greater off-rate for glycine than has the wild-type variant; that is, the glycine inhibition constant (K_i) for the soluble NR1 S1S2 Y535S mutant is roughly 2.5-fold higher than that for the wild-type construct (Supplementary Fig. S4). Because most NR1–NR2A receptors are present in a non-desensitized state after a brief (1–5 ms) application of ligand, dissociation (rather than entry and residence in the desensitized state) is most probably the main determinant of the deactivation rate in this case[12,40].

To explore the dependence of glycine and glutamate deactivation rates on the nature of the side chain at residue 535 of NR1, we examined the Y535L and Y535F mutants. Substitution of the aromatic ring by an aliphatic side chain in the Y535L mutant yields only a modest increase in the rates of glycine and glutamate deactivation, primarily owing to an increase in the weight of the fast component with no significant difference in τ_f and τ_s (Fig. 6c, d). This result underscores the importance of a planar, aromatic ring at position 535. In the crystal structures, the planar ring of aniracetam in GluR2 and Y535 in NR1 interact with conserved prolines (P494 in GluR2, P532 in NR1 and P527 in NR2A) through van der Waals contacts (Fig. 5c), interactions that are apparently crucial for slowing deactivation. Such interactions are absent in the rapidly deactivating non-NMDA receptors, which have small and hydrophilic residues (S497 in GluR2 and T504 in GluR6) at the position equivalent to Y535 in NR1. To a large extent, an aromatic residue at position 535 is important for maintaining the slow component of receptor deactivation. Accordingly, the Y535F mutant shows slightly slower deactivation rates and has weights for the fast and slow components similar to those of the wild-type receptor. This mutant also suggests that the hydroxyl group of NR1 Y535 and the two water-mediated hydrogen bonds (Fig. 5b, c) are not crucial in modulating the rate of receptor deactivation.

The tryptophan mutant, Y535W, has an aromatic side chain similar in size to aniracetam and shows two opposing effects: on the one hand, it slows the rate of glutamate-dependent deactivation by ~2-fold; on the other, it increases the rate of the glycine-dependent deactivation by ~2.6-fold (Fig. 6). If a tryptophan is modelled at position 535, the indole ring makes additional hydrophobic contacts with NR1 P532 and NR2A P527, and these contacts may stabilize the NR2A clam shell in a closed-cleft, activated conformation more effectively than does tyrosine. Why then does the tryptophan mutation speed the rate of glycine-dependent deactivation? Inspection of the open-cleft, antagonist-bound structure of NR1 S1S2[28] superimposed onto the glycine-bound NR1 subunit in the NR1–NR2A complex shows that the tyrosine occupies a different position in the antagonist-bound form owing to movement of the Cγ atom by ~1.6 Å and rotation of the Cδ–Cγ–Cβ–Cα dihedral angle by ~25°. Therefore, either the tryptophan may stabilize the NR1 glycine-binding domain in an open cleft conformation, perhaps by interactions with I755 of NR2A, or it may simply destabilize the closed-cleft state.

Conclusion

This study defines the NR1–NR2 S1S2 heterodimer as the fundamental functional unit in NR1–NR2A NMDA receptors and, together with previous studies, shows that the agonist-binding domains of NMDA and non-NMDA receptors are organized as dimeric units. This conservation of architecture in turn suggests the conservation of a gating mechanism in which the agonist-induced closure of each ligand-binding domain results in separation of the ion channel proximal portions of the receptors (the 'linkers') and opening of the ion permeation pathway. Lastly, in both NMDA and non-NMDA receptors, the dimer interface provides sites for the allosteric modulation of gating activity.

METHODS

Structure determination. All data sets were collected on beam line X4A at the National Synchrotron Light Source using a Quantum 4 charged-coupled device detector (ADSC). The data sets were indexed, scaled and merged with HKL2000[41]. The rat NR2A S1S2 structure was determined by combining phases from single-wavelength anomalous dispersion (SAD) data collected on an NaBr-soaked crystal at the bromine peak energy and from molecular replacement using the Cα coordinates for domain 1 of the rat NR1 S1S2–glycine structure without loops 1 and 2 (T396–V409, C454–Q487, E497–Q536 and S756–S800) as a search probe. The bromide sites were found with SOLVE[42] and molecular replacement was done with AmoRe[43]. Phase combination and extension were accomplished with SIGMAA[44] and DM[45], respectively. We determined the NR1–NR2A S1S2 structure by molecular replacement using a heterodimer search probe model built by superposing the structures of NR1 S1S2–glycine[28] and NR2A S1S2–glutamate onto the GluR2 S1S2 dimer structure in helix J.

Refinement was done with CNS[46]. Iterative rounds of model building in the program O[47] were carried out by using $F_o - F_c$ omit maps, coupled with Powell minimization and individual *B*-factor refinement, until R_{free} converged. When R_{free} was below 30%, ligands (glycine for NR1 and glutamate for NR2A) and water molecules were added, and the model was further refined until R_{free} converged again.

Electrophysiology. Oocyte recordings of the rat NR1–NR2A NMDA receptors were done in a TEVC configuration by using agarose-tipped microelectrodes filled with 3 M KCl at a holding potential of −60 mV. The bath solution contained 5 mM HEPES, 100 mM NaCl, 2.8 mM KCl, 10 mM Tricine and 0.3 mM $BaCl_2$ (pH 7.3).

For the fast-perfusion experiments, HEK293 cells (TsA201 variant) attached to 12-mm poly-D-lysine coated glass coverslips were transfected with plasmids encoding NR1-1a (rat), NR2A (rat) and green fluorescent protein using Lipofectamine2000 (Invitrogen). Recordings were made 24–36 h after transfection at room temperature with an Axopatch 200B amplifier (Axon Instruments). Recording electrodes (3–6 MΩ) were filled with 110 mM potassium gluconate, 2.5 mM NaCl, 5 mM BAPTA and 10 mM HEPES-KOH (pH 7.4). The wash solution contained 150 mM NaCl, 2.5 mM KCl, 2 mM $CaCl_2$, 10 mM HEPES-NaOH (pH 7.4), 10 mM glucose, 10 mM Tricine and 0.1 mM glycine or glutamate. The ligand solution contained wash solution plus 1 mM of glutamate or glycine and 5 mM sucrose to increase visibility of the solution interface. The outside-out patch was placed in front of the double-barrel theta tubing mounted on a piezoelectric device (Burleigh). The mean 10–90% rise time for the open tip response was typically 500–1,000 μs. Brief (3-ms) pulses of the ligand solutions were applied and 20–50 recordings were obtained at 5-s intervals at a holding potential of −70 mV. The data points were averaged and fitted with a double exponential equation, $I(t) = I_f \times \exp(-t/\tau_f) + I_s \times \exp(-t/\tau_s)$, where I_f and I_s are the amplitudes of the fast and slow decay components and τ_f and τ_s are their respective decay time constants used to fit the data. We calculated the weighted mean decay time constant by the formula: $\tau_w = I_f/(I_f + I_s) \times \tau_f + I_s/(I_f + I_s) \times \tau_s$.

Analytical ultracentrifugation. Sedimentation equilibrium experiments were done in a Beckman Coulter Optima XL-I analytical ultracentrifuge with absorbance optics and quartz windows. Before these runs, protein samples were purified by Superdex 200 gel filtration chromatography, concentrated and dialysed overnight against a buffer containing 20 mM sodium phosphate (pH 7.5), 150 mM NaCl, 1 mM EDTA and either 1 mM glycine (NR1 S1S2 variants) or 1 mM L-glutamate (NR2A S1S2 variants). The mixture was made by combining equimolar amounts of mutant NR1 and NR2A and then dialysing it overnight against the same buffer containing both 1 mM glycine and 1 mM L-glutamate.

Protein samples were loaded into six-sector, 12-mm charcoal-filled Epon centrepieces at 0.1, 0.2, 0.4, 0.8, 1.0 and 1.2 mg ml^{-1} and run at 13,000, 18,000, and 25,000 r.p.m. in an An50Ti rotor at 4 °C. We collected absorbance (280-nm) scans at 2-h intervals with a 0.001-cm spacing and ten replicates per point. Data were analysed by nonlinear regression in WinNONLIN[48]. Solvent density and viscosity were calculated with Sednterp[49]. Association constants for any monomer–dimer equilibria obtained from WinNONLIN were converted from absorbance ($K_{2,abs}$) to molar units ($K_{2,M}$) with the equation $K_{2,M} = K_{2,abs}(\varepsilon l)/2$, where *l* is the path

length of the cell (1.2 cm) and ε is the molar extinction coefficient at 280 nm (36,840 and 32,430 $M^{-1} cm^{-1}$, respectively, for NR1 and NR2A, estimated from the amino acid sequences disregarding disulphide bonds).

Received 2 June; accepted 20 July 2005.

1. Kandel, E. R., Schwartz, J. H. & Jessel, T. M. *Essentials of Neural Science and Behavior* 219–306 (Appleton & Lange, East Norwalk, Connecticut, 1995).
2. Watkins, J. C. & Evans, R. H. Excitatory amino acid transmitters. *Annu. Rev. Pharmacol. Toxicol.* **21,** 165–204 (1981).
3. Hollmann, M., O'Shea-Greenfield, A., Rogers, S. W. & Heinemann, S. Cloning by functional expression of a member of the glutamate receptor family. *Nature* **342,** 643–648 (1989).
4. Keinänen, K. *et al.* A family of AMPA-selective glutamate receptors. *Science* **249,** 556–560 (1990).
5. Boulter, J. *et al.* Molecular cloning and functional expression of glutamate receptor subunit genes. *Science* **249,** 1033–1037 (1990).
6. Werner, P., Voigt, M., Keinänen, K., Wisden, W. & Seeburg, P. H. Cloning of a putative high-affinity kainate receptor expressed predominantly in hippocampal CA3 cells. *Nature* **351,** 742–744 (1991).
7. Moriyoshi, K. *et al.* Molecular cloning and characterization of the rat NMDA receptor. *Nature* **354,** 31–37 (1991).
8. Johnson, J. W. & Ascher, P. Glycine potentiates the NMDA response in cultured mouse brain neurons. *Nature* **325,** 529–531 (1987).
9. Mayer, M. L., Westbrook, G. L. & Guthrie, P. B. Voltage-dependent block by Mg^{2+} of NMDA responses in spinal cord neurones. *Nature* **309,** 261–263 (1984).
10. MacDermott, A. B., Mayer, M. L., Westbrook, G. L., Smith, S. J. & Barker, J. L. NMDA-receptor activation increases cytoplasmic calcium concentration in cultured spinal cord neurones. *Nature* **321,** 519–522 (1986).
11. Forsythe, I. D. & Westbrook, G. L. Slow excitatory postsynaptic currents mediated by *N*-methyl-D-aspartate receptors on cultured mouse central neurones. *J. Physiol.* **396,** 515–533 (1988).
12. Vicini, S. *et al.* Functional and pharmacological differences between recombinant *N*-methyl-D-aspartate receptors. *J. Neurophysiol.* **79,** 555–566 (1998).
13. Lester, R. A., Clements, J. D., Westbrook, G. L. & Jahr, C. E. Channel kinetics determine the time course of NMDA receptor-mediated synaptic currents. *Nature* **346,** 565–567 (1990).
14. Cull-Candy, S., Brickley, S. & Farrant, M. NMDA receptor subunits: diversity, development and disease. *Curr. Opin. Neurobiol.* **11,** 327–335 (2001).
15. Waxman, E. A. & Lynch, D. R. *N*-methyl-D-aspartate receptor subtypes: multiple roles in excitotoxicity and neurological disease. *Neuroscientist* **11,** 37–49 (2005).
16. Benveniste, M. & Mayer, M. L. Kinetic analysis of antagonist action at *N*-methyl-D-aspartic acid receptors. Two binding sites each for glutamate and glycine. *Biophys. J.* **59,** 560–573 (1991).
17. Clements, J. D. & Westbrook, G. L. Activation kinetics reveal the number of glutamate and glycine binding sites on the *N*-methyl-D-aspartate receptor. *Neuron* **7,** 605–613 (1991).
18. Watanabe, M., Inoue, Y., Sakimura, K. & Mishina, M. Developmental changes in distribution of NMDA receptor channel subunit mRNAs. *Neuroreport* **3,** 1138–1140 (1992).
19. Monyer, H., Burnashev, N., Laurie, D. J., Sakmann, B. & Seeburg, P. H. Developmental and regional expression in the rat brain and functional properties of four NMDA receptors. *Neuron* **12,** 529–540 (1994).
20. Laurie, D. J. & Seeburg, P. H. Ligand affinities at recombinant *N*-methyl-D-aspartate receptors depend on subunit composition. *Eur. J. Pharmacol.* **268,** 335–345 (1994).
21. Erreger, K., Chen, P. E., Wyllie, D. J. & Traynelis, S. F. Glutamate receptor gating. *Crit. Rev. Neurobiol.* **16,** 187–224 (2004).
22. Ayalon, G. & Stern-Bach, Y. Functional assembly of AMPA and kainate receptors is mediated by several discrete protein-protein interactions. *Neuron* **31,** 103–113 (2001).
23. Armstrong, N. & Gouaux, E. Mechanisms for activation and antagonism of an AMPA-sensitive glutamate receptor: crystal structures of the GluR2 ligand binding core. *Neuron* **28,** 165–181 (2000).
24. Sun, Y. *et al.* Mechanism of glutamate receptor desensitization. *Nature* **417,** 245–253 (2002).
25. Schorge, S. & Colquhoun, D. Studies of NMDA receptor function and stoichiometry with truncated and tandem subunits. *J. Neurosci.* **23,** 1151–1158 (2003).
26. Meddows, E. *et al.* Identification of molecular determinants that are important in the assembly of N-methyl-D-aspartate receptors. *J. Biol. Chem.* **276,** 18795–18803 (2001).
27. Regalado, M. P., Villarroel, A. & Lerma, J. Intersubunit cooperativity in the NMDA receptor. *Neuron* **32,** 1085–1096 (2001).
28. Furukawa, H. & Gouaux, E. Mechanisms of activation, inhibition and specificity: crystal structures of the NMDA receptor NR1 ligand-binding core. *EMBO. J.* **22,** 2873–2885 (2003).
29. Inanobe, A., Furukawa, H. & Gouaux, E. Mechanism of partial agonist action at the NR1 subunit of NMDA receptors. *Neuron* **47,** 71–84 (2005).
30. Jin, R., Horning, M., Mayer, M. L. & Gouaux, E. Mechanism of activation and selectivity in a ligand-gated ion channel: structural and functional studies of GluR2 and quisqualate. *Biochemistry* **41,** 15635–15643 (2002).
31. Armstrong, N., Sun, Y., Chen, G. Q. & Gouaux, E. Structure of a glutamate-receptor ligand-binding core in complex with kainate. *Nature* **395,** 913–917 (1998).
32. Mayer, M. L. Crystal Structures of the GluR5 and GluR6 ligand binding cores: molecular mechanisms underlying kainate receptor selectivity. *Neuron* **45,** 539–552 (2005).
33. Nanao, M. H., Green, T., Stern-Bach, Y., Heinemann, S. F. & Choe, S. Structure of the kainate receptor subunit GluR6 agonist-binding domain complexed with domoic acid. *Proc. Natl Acad. Sci. U S A* **102,** 1708–1713 (2005).
34. Laube, B., Schemm, R. & Betz, H. Molecular determinants of ligand discrimination in the glutamate-binding pocket of the NMDA receptor. *Neuropharmacology* **47,** 994–1007 (2004).
35. Watkins, J. C., Krogsgaard-Larsen, P. & Honore, T. Structure-activity relationships in the development of excitatory amino acid receptor agonists and competitive antagonists. *Trends Pharmacol. Sci.* **11,** 25–33 (1990).
36. Choi, Y., Chen, H. V. & Lipton, S. A. Three pairs of cysteine residues mediate both redox and Zn^{2+} modulation of the NMDA receptor. *J. Neurosci.* **21,** 392–400 (2001).
37. Folta-Stogniew, E. & Williams, K. R. Determination of molecular masses of proteins in solution: implementation of an HPLC size exclusion chromatography and laser light scattering service in a core laboratory. *J. Biomol. Technol.* **10,** 51–63 (1999).
38. Stern-Bach, Y., Russo, S., Neuman, M. & Rosenmund, C. A point mutation in the glutamate binding site blocks desensitization of AMPA receptors. *Neuron* **21,** 907–918 (1998).
39. Jin, R. *et al.* Mechanism of positive allosteric modulators acting on AMPA receptors. *J. Neurosci.* **25,** 9027–9036 (2005).
40. Erreger, K., Dravid, S. M., Banke, T. G., Wyllie, D. J. & Traynelis, S. F. Subunit-specific gating controls rat NR1/NR2A and NR1/NR2B NMDA channel kinetics and synaptic signalling profiles. *J. Physiol.* **563,** 345–358 (2005).
41. Otwinowski, Z. & Minor, W. Processing of X-ray diffraction data collected in oscillation mode. *Methods Enzymol.* **276,** 307–326 (1997).
42. Terwilliger, T. C. & Berendzen, J. Automated MAD and MIR structure solution. *Acta Crystallogr. D* **55,** 849–861 (1999).
43. Navaza, J. *Amore*: An automated package for molecular replacement. *Acta Crystallogr. A* **50,** 157–163 (1994).
44. Read, R. J. Improved Fourier coefficients for maps using phases from partial structures with errors. *Acta Crystallogr. A* **42,** 140–149 (1986).
45. Cowtan, K. D. & Main, P. Phase combination and cross validation in iterated density-modification calculations. *Acta Crystallogr. D Biol. Crystallogr.* **52,** 43–48 (1996).
46. Brunger, A. T. *et al.* Crystallography & NMR system: A new software suite for macromolecular structure determination. *Acta Crystallogr. D* **54(** 5), 905–921 (1998).
47. Jones, T. A. & Kjeldgaard, M. Electron-density map interpretation. *Methods Enzymol.* **277,** 173–208 (1997).
48. Yphantis, D., Johnson, M. L. & Lary, J. W. *WinNONLIN106* program. (National Analytical Ultracentrifugation Facility, Univ. Connecticut, Storrs, CT, 1997).
49. Schuck, P. Size-distribution analysis of macromolecules by sedimentation velocity ultracentrifugation and lamm equation modeling. *Biophys. J.* **78,** 1606–1619 (2000).
50. Kabsch, W. A solution for the best rotation to relate two sets of vectors. *Acta Crystallogr. A* **32,** 922–923 (1976).

Supplementary Information is linked to the online version of the paper at www.nature.com/nature.

Acknowledgements We are grateful to A. Rowe for comments on the sedimentation equilibrium data analysis. M. Mayer is thanked for discussions, critical reading of this manuscript, and pSP NR1-1a and NR2A. J. Howe and S. Traynelis are thanked for comments on electrophysiological experiments and for the TsA201 cell-line and pCINEO NR1-1a and NR2A, respectively. We thank N. Armstrong, W. Zhang, and A. Robert for instructions on the patch-clamp and rapid solution exchange experiments; R. Abramowitz and X. Yang for assistance with the X-ray experiments; S. Siegelbaum for providing *Xenopus* oocytes; and A. Sobolevsky and O. Boudker for critically reading the manuscript. The NR1 and NR2A cDNAs used in the structural analysis were a gift from S. F. Heinemann. S.K.S is supported by an NIH National Research Service Award postdoctoral fellowship. The Beckman XL-I analytical centrifuge was purchased with funds from the NIH. The work was supported by the NIH. E.G. is an investigator with the Howard Hughes Medical Institute.

Author Information The coordinates and structure factors for NR1–NR2A S1S2 and NR2A S1S2–glutamate have been deposited in the Protein Data Bank with accession codes 2A5T and 2A5S, respectively. Reprints and permissions information is available at npg.nature.com/reprintsandpermissions. The authors declare no competing financial interests. Correspondence and requests for materials should be addressed to E.G. (jeg52@columbia.edu).